J. Fluid Mech. (1999), *vol.* 384, *pp.* 133–158. Printed in the United Kingdom

© 1999 Cambridge University Press

Experimental study of the sedimentation of dilute and semi-dilute suspensions of fibres

By BENJAMIN HERZHAFT† AND ÉLISABETH GUAZZELLI‡

Laboratoire de Physique et Mécanique des Milieux Hétérogènes, UMR 7636 du CNRS, ESPCI, 10 rue Vauquelin, 75231 Paris CEDEX 05, France

(Received 3 April 1998 and in revised form 26 October 1998)

Steady-state velocity and orientation distributions of sedimenting fibres were measured as a function of particle concentration and aspect ratio. Two different regimes of sedimentation were clearly identified. For dilute suspensions, the fibres tend to align in the direction of gravity with occasional flipping and clump together to form packets. In this regime, the vertical mean sedimentation speed is not hindered and can be larger than the Stokes' velocity of an isolated vertical fibre. Its scaling is a complex function of particle volume fraction and aspect ratio. As the concentration is increased, the fibres still tend to orient in the direction of gravity. The mean velocity becomes hindered and scales with particle volume fraction. The velocity fluctuations were found to be large and anisotropic. They were found to increase with increasing volume fraction. A similar substantial anisotropy of the orientation distribution was observed for all particle concentrations and aspect ratios studied.

1. Introduction

The sedimentation of solid particles is found in a variety of natural phenomena such as the flow of sediment in rivers and estuaries or the sedimentation of rain drops and dust in the atmosphere. Sedimentation is also used in industry as an inexpensive way to clarify liquids (or alternatively to recover particles) as well as to separate particles of different densities or sizes. Despite the longstanding use of sedimentation in practical applications, much remains unknown about the fundamental properties of sedimenting suspensions such as the mean sedimenting velocity and the dispersion (or mixing) of particles due to velocity fluctuations. The problem that one encounters in the determination of these properties lies in the long-range nature of multibody hydrodynamic interactions between particles. Another difficulty is that these properties are strongly dependent on the microstructure of the suspension, i.e. the orientations and relative positions of the particles, which, itself, is usually determined by these interactions. These two separate issues make the sedimentation problem particularly difficult. In this paper, we will consider suspensions composed of non-Brownian rigid particles sedimenting in a Newtonian fluid under Stokes' flow conditions.

† Present address: Institut Français du Pétrole, 1–4 Avenue de Bois-Préau, BP311, 92506 Rueil-Malmaison Cedex, France.

‡ Present address: Institut Universitaire des Systèmes Thermiques Industriels, UMR 6595 du CNRS, Technopôle de Château-Gombert, 5 rue Enrico Fermi, 13453 Marseille Cedex 13, France.

The most studied sedimenting system is a monodisperse suspension of spheres. In the absence of hydrodynamic interactions, i.e. in the infinitely dilute case, particles sediment at the Stokes' velocity

$$\boldsymbol{V}_S^{sphere} = \frac{\Delta\rho d_p^2}{18\eta}\boldsymbol{g}, \tag{1.1}$$

where d_p is the sphere diameter, $\Delta\rho = \rho_p - \rho_f$ is the difference between the density of the particles and that of the fluid, η is the fluid viscosity, and $\boldsymbol{g}$ is the acceleration due to gravity. As the concentration is increased, hydrodynamic interactions lead to a decrease in the settling velocity relative to $\boldsymbol{V}_S^{sphere}$, in particular through the effect of the fluid backflow, see for instance the review of Davis & Acrivos (1985). The mean sedimentation velocity, $\langle \boldsymbol{V} \rangle$, can be expressed in terms of the hindrance function $f(c)$ by

$$\langle \boldsymbol{V} \rangle = f(c)\boldsymbol{V}_S^{sphere} \tag{1.2}$$

where c is the particle volume fraction. Here and in the remainder of the paper, the brackets $\langle\ \rangle$ denote an ensemble average. The suspension structure, i.e. the details of the relative positions of the spheres, has a strong effect on the departure of $f(c)$ from unity, see Saffman (1973). Even in the dilute case (first correction to the Stokes' velocity), the prediction for a regular array of spheres is of the form $f(c) = 1 - O(c^{1/3})$, see Hasimoto (1959) and Sangani & Acrivos (1982), while that for free randomly positioned spheres is $f(c) = 1 - O(c)$, see Batchelor (1972). This latter case, which is supposed to be the one most likely to occur in practice, has been the subject of many theoretical studies, see for instance the review of Davis & Acrivos (1985). On the experimental side, the most commonly found empirical correlation is that attributed to Richardson & Zaki (1954), $f(c) = (1 - c)^n$, with an exponent $n \approx 5$ at small Reynolds numbers which differs from the $O(c)$ coefficient of Batchelor (1972) in the dilute limit ($= 6.55$). The actual structure of the suspension is determined by the hydrodynamic interactions in the non-Brownian suspensions considered here. While the suspension is certainly not spatially periodic, the question remains whether it is completely random.

Understanding the microstructure is even more crucial for the determination of the velocity fluctuations. The fluctuations in the velocity of the particles are due to the constantly changing configuration of the suspension microstructure. These fluctuations have been found experimentally to be very large, $O(\langle V \rangle)$, and to have a diffusive longtime behaviour known as hydrodynamic diffusion with self-diffusivities $O(\langle V \rangle d_p/2)$, see Ham & Homsy (1988), Xue *et al.* (1992), and Nicolai *et al.* (1995). However, at the present time, there remains a serious theoretical problem regarding the amplitude of these fluctuations. While analytical calculations for a dilute random suspension by Caflisch & Luke (1985) and Hinch (1988) as well as numerical simulations by Koch (1994), Da Cunha (1994) and Ladd (1997) predict that the fluctuations diverge as the size of the container is increased, no such evidence is found in the experiments (see, for instance, Nicolai & Guazzelli 1995 and Segrè, Helbolzheimer & Chaikin 1997) and the screening theory of Koch & Shaqfeh (1991). The main finding of the recent experiments of Segrè, Herbolzheimer & Chaikin (1997) is that the fluctuations form into characteristic correlated regions having a size of approximately 20 mean interparticle distances. The origin of this particular length scale is still an open question. In summary, although there has been significant progress in the understanding of the sedimentation velocity of spherical particles, there are still

some remaining problems particularly concerning the velocity fluctuations and the detailed knowledge of the suspension microstructure.

Understanding the sedimentation of non-spherical particles is an even more difficult task. In this case, the suspension structure has an even greater influence on the sedimentation velocity. In the present work, we shall confine our attention to suspensions composed of rod-like particles, although disk-like particles are also still in need of further studies. In the absence of hydrodynamic interactions, the sedimentation velocity of a fibre of length l_p and diameter d_p (with an aspect ratio $r = l_p/d_p$) can be written with the use of slender body theory as

$$\boldsymbol{V}_S^{fibre} = \frac{\Delta\rho(d_p)^2}{16\eta}[(\ln 2r + 0.193 + O(\ln 2r)^{-1})\boldsymbol{g} + (\ln 2r - 1.807 + O(\ln 2r)^{-1})(\boldsymbol{p}\cdot\boldsymbol{g})\boldsymbol{p}], \tag{1.3}$$

see Batchelor (1970), Mackaplow (1996), and Mackaplow & Shaqfeh (1998), where the fibre director $\boldsymbol{p}$ is the unit vector that indicates its orientation. Unlike spheres, isolated fibres can have motion perpendicular to gravity. Both velocities parallel and perpendicular to gravity strongly depend on the fibre orientation. For example, a high aspect ratio fibre aligned with gravity settles about twice as fast as when it is perpendicular to gravity. Therefore the mean sedimentation velocity in a suspension of fibres depends drastically on the fibre orientation distribution. Each fibre settles and rotates under the influence of the long-range fluid disturbances resulting from the settling of the surrounding fibres. The fibre orientation distribution is entirely determined by these interparticle hydrodynamic interactions. This is also the case for fibres in other simple flows such as shear flow and flow through fixed beds, see for instance Shaqfeh & Koch (1988) and Rahnama, Koch & Shaqfeh (1995). In the present sedimentation case, the orientation distribution is coupled to the velocity of the fibre centre of mass and changes in this distribution can produce $O(1)$ change in the settling velocity. Because of these difficulties, the existing theoretical and experimental work on the sedimentation of fibres is recent and extremely limited. Theoretical studies have been confined to dilute suspensions while the dilute and semi-dilute regimes of sedimentation have been examined experimentally.

Before summarizing the existing literature, let us define the different regimes, see for example the review of Blanc (1995). Since fibres disturb the surrounding fluid over lengths of the order l_p, it is usual to define an effective particle volume fraction, $n(l_p/2)^3$, in terms of the interaction length, $l_p/2$, and the number of particles per unit volume, n. The case of dilute suspension corresponds to $n(l_p/2)^3 \ll 1$ for which, on average, each fibre occupies a large volume in which it can freely rotate. The semi-dilute regime is reached for $n(l_p/2)^3 \gg 1 \gg n(l_p/2)^2(d_p/2)$. The suspension becomes concentrated only when $n(l_p/2)^2(d_p/2) \approx 1$, which may correspond to a rather small fibre volume fraction c. Another dimensionless number which can be constructed with n, l_p, and d_p is $n(l_p/2)(d_p/2)^2$ and is proportional to the fibre volume fraction, $c = 2\pi n(l_p/2)(d_p/2)^2$. The last dimensionless number which can be constructed is $n(d_p/2)^3$ and has little known importance.

Most previous fibre experiments have been confined to the measurement of the settling speed of the interface between the clear fluid and the suspension which happens to be rather diffuse in settling suspensions of fibres. Turney *et al.* (1995) examined the sedimentation of rod-like particles with a single aspect ratio ($r = 17.4$) using magnetic resonance imaging. Their results, all within the semi-dilute regime of particle concentration, show a larger hindered settling effect with increasing particle

volume fractions than that found for spherical particles. Anselmet (1989) measured the velocity of individual fibres in the dilute regime and the interface speed for larger concentrations using optical techniques. Her results show two distinct regimes of hindered settling as a function of volume fractions for fibres with $r \approx 10$. The results seemed to be independent of r when it was varied from 5 to 17. Anselmet (1989)'s data are however lower than those of Turney *et al.* (1995), this discrepancy being attributed to the small size of her settling vessel. However, these experimental studies do not provide any information about the orientation distribution, except at the initial state for which it is considered isotropic.

Conversely, Herzhaft *et al.* (1996) measured the centre-of-mass velocities and orientations of sedimenting marked fibres in an otherwise index-matched settling fibre suspension. Their results, for a single concentration in the dilute regime ($n(l_p/2)^3 \approx 10\%$) and for $r \approx 10$, show that the suspension reaches a steady state where the fibres 'clump' together to form packets and tend to align in the direction of gravity with occasional flipping motions between the two gravitationally aligned orientations. The large shear stresses between the different sparse and dense regions of the suspension were considered to be the cause of the flipping motions. The mean sedimentation velocity was found to be not hindered at all but, in fact, to be larger than the maximum possible value for an isolated particle, i.e. the Stokes' velocity of a vertical fibre. Indeed, fibre packets settle faster than isolated vertical fibres. In contrast with the previous experimental results, these recent observations show that the sedimentation of fibres is qualitatively different to the sedimentation of spheres. We should mention that the existence of fibre packets settling at large velocities was also reported by Kumar & Ramarao (1991) for long glass fibres sedimenting in an aqueous glycerol solution at low volume fractions. Kumar & Ramarao (1991) also noted that, as the fibre concentration increased, the number of packets (called 'flocs' by these authors) increased and caused hindrance effects and that, for even larger concentrations, the settling speed was then governed by the network of fibres that was formed and dropped abruptly.

The experimental findings of Herzhaft *et al.* (1996) are consistent with the results of the linear stability analysis of Koch & Shaqfeh (1989) who demonstrated that, unlike a suspension of spheres, a settling homogeneous suspension of spheroids can be unstable precisely because of the coupling between the orientation distribution and the centre-of-mass velocities and that it then evolves to an inhomogeneous settling state in which the inhomogeneities cause the mean sedimentation velocity to be larger than the maximum possible value for an isolated fibre. However, at the present time, there are no theoretical predictions of the steady-state mean sedimentation velocity and orientation distribution achieved by a settling suspension of fibres. Claeys & Brady (1993) computed the concentration dependence of the sedimentation rate of crystalline suspensions using Stokesian dynamics numerical simulations. Mackaplow & Shaqfeh (1998) performed a full finite-length-fibre numerical simulation and found, for homogeneous suspensions with isotropic orientation distributions, that the mean sedimentation velocity is hindered in good agreement with the prediction of a dilute theory corrected for the effects of two-body interactions and with the experimental results of Turney *et al.* (1995).

These two numerical simulations assumed a particular orientation and centre-of-mass distributions of the fibres. In contrast, in a second study, Mackaplow & Shaqfeh (1998) have attempted to determine the evolution of the orientation and velocity distributions in a dilute sedimenting suspension of point fibres, i.e. in which the hydrodynamic interactions are limited to point interactions while the 'orientation' of the points can vary. They found that the fibres tend to orient and to cluster into

long 'streamers' in the direction of gravity. The degree of vertical orientation was found to be less in the simulations than in the experiments of Herzhaft *et al.* (1996). Flipping motions were observed in the simulations in qualitative agreement with the experiments. However, unlike in the experiments where a steady state was reached, a continued linear increase of the mean velocity with time as well as a continued fibre clustering was found in the simulations.

To summarize the existing experimental literature, Herzhaft *et al.* (1996) have discovered a dilute regime of inhomogeneous sedimentation in which the fibres tend to align in the direction of gravity and to clump together in packets. It is now necessary to identify more precisely this regime and to understand the fibre clumping mechanism. It is also fundamental to examine whether this packet instability still exists at larger volume fractions and how the fibre aspect ratio influences the instability growth. The previous experimental studies of Turney *et al.* (1995) and Anselmet (1989) have found that sedimentation is greatly hindered at larger volume fractions. However, since the structure of the suspension and, in particular, the fibre orientation was not measured in these experiments, it is difficult to determine whether they represent steady-state results.

It is therefore important to measure both the velocity and orientation distributions in the bulk of a sedimenting suspension for volume fractions ranging from the dilute to the semi-dilute regimes. This is precisely the objective of the present work. To this end, a few marked glass fibres were tracked in the midst of a suspension of unmarked like fibres, made optically transparent by matching the index of refraction of the suspending fluid to that of the fibres. Both the location of the centre of mass and the orientation of the marked fibres were measured during the sedimentation process. This fibre tracking technique, used by Herzhaft *et al.* (1996), has been derived from that developed by Nicolai *et al.* (1995) for the sedimentation of spheres. Steady-state mean sedimentation velocities, root mean squares of the fluctuations, and orientation distributions were measured as a function of fibre concentration and aspect ratio. Visualizations of the suspension structure were also undertaken. The long-time behaviour of the fluctuating fibre motions was examined in the dilute regime. Some correlation functions were measured. This provided information about the time scale over which hydrodynamic interactions affect the orientation distribution and the hydrodynamic diffusion of the centre of mass. The paper is organized as follows. The experimental techniques are presented in § 2. The experimental results are given in § 3 and discussed in § 4.

2. Experimental techniques

2.1. *Suspensions*

The particles were glass rods specially manufactured by Mo-Sci Corporation (Rolla, Missouri, USA) with index of refraction 1.473 ± 0.001. The rods were cylindrical, except for some roughness at the end. Four batches of fibres with different aspect ratios were used. The fibre length and diameter distributions were obtained from measurements of 800 rods for the first batch, 600 rods for the second batch, and 400 rods for the two last batches with a charged coupled device camera and a digital imaging system (see § 2.2). The distributions were found to be approximately Gaussian and the mean and standard deviations were determined. The fibre length, l_p, and diameter, d_p, are given in table 1. The error in length (or diameter) is one standard deviation of the size distribution. The fibre density was determined, using

Batch	l_p (cm)	d_p (cm)	r	$V_{S\parallel}$ (cm s^{-1})
1	0.11 ± 0.02	0.0101 ± 0.0006	11 ± 2	0.006 ± 0.001
2	0.29 ± 0.02	0.0090 ± 0.0008	32 ± 4	0.007 ± 0.001
3	0.19 ± 0.02	0.010 ± 0.001	20 ± 3	0.007 ± 0.002
4	0.05 ± 0.02	0.010 ± 0.001	5 ± 2	0.004 ± 0.001

TABLE 1. Properties of the fibres.

Archimedes' principle, by measuring the volume variation when a weighted amount of fibres was introduced in a given volume of distilled water in a graduated vessel. The different fibres have the same density within error bars, $\rho_p = 2.2 \pm 0.1$ g cm^{-3}. A fraction of the fibres was uniformly silvered so that they could be tracked in the midst of an optically transparent sedimenting suspension of like particles. The silvering process was performed by reduction of an ammonia solution of silver nitrate by an alcoholic solution of saccharose. The thin coating of silver did not modify the particle settling characteristics, as we verified experimentally by measuring the velocity of isolated fibres.

The fluid was viscous enough to maintain creeping flow conditions and to have the same index of refraction as that of the glass rods so that the suspensions would be optically transparent. The fluid selected was an organic mixture of 15% Santicizer 97 and 85% Santicizer 431 (both produced by Monsanto). The matching of the refractive index of the fluid with that of the glass rods of the suspension was ensured by air-conditioning the laboratory room at $22 \pm 1^\circ$ C. At this temperature, the fluid viscosity was $\eta = 5.5 \pm 0.5$ P and the fluid density was $\rho_f = 1.07 \pm 0.01$ g cm^{-3}. The fluid viscosity was measured with a rheometer, and its Newtonian behaviour was also verified.

For these two combinations of fluid and fibres, the fibre Reynolds number defined as $l_p V_{S\parallel} \rho_f / \eta$ was smaller than 10^{-4} where $V_{S\parallel}$ is the theoretical value of the Stokes' velocity of an isolated vertically oriented fibre, i.e. the maximum velocity that an isolated fibre can achieve. In order to normalize the measured velocities (see § 3), we chose to use Batchelor's third-order asymptotic result (provided for each batch in table 1)

$$V_{S\parallel} = V_{S\parallel}^{fibre} = \frac{\Delta\rho g (d_p)^2}{16\eta} [2 \ln 2r - 1.614 - 0.355(\ln 2r)^{-1} + O(\ln 2r)^{-2}], \qquad (2.1)$$

see Batchelor (1970), Mackaplow (1996), and Mackaplow & Shaqfeh (1998). The difference between Batchelor's results and the numerical results of Youngren & Acrivos (1975) is smaller than 3% for $r \geqslant 10$. There is a 10% difference between the two results at $r = 5$, which lies within the experimental error bar. The Brownian Péclet number, $l_p V_{S\parallel} / 2D_{cm}$, where D_{cm} is the centre-of-mass Brownian diffusivity, was always very large. The effect of fibre bending can also be estimated. It is maximum when the fibre is oriented perpendicular to gravity. Using slender body theory, see Batchelor (1970) and Mackaplow (1996), the maximum bending moment operating along the fibre axis can be computed. Saint-Venant's theorem is then applied to compute the minimum radius of curvature $= O(E / g r^2 \Delta\rho)$ where E is the modulus of elasticity. For the fibres considered here, this radius was always much larger than the fibre length. Thus, the effect of inertial forces, Brownian forces, and fibre bending were negligible under the experimental conditions.

The suspensions were contained in a glass-walled cell of rectangular cross-section with an inside width of 10.00 ± 0.05 cm, an inside depth of 8.00 ± 0.05 cm and a height of 50.00 ± 0.05 cm. Russel *et al.* (1977) have shown that the motion of a fibre is influenced by a vertical wall over distances smaller than approximately $6l_p$. The present vessel was thus sufficiently large ($73l_p$ for the first batch and $28l_p$ for the second batch in the smallest dimension) for considering measurements in the middle region of the cell as representative of bulk suspension measurements (see § 2.2). Experiments were carried out by introducing weighed amounts of fluid and silvered and unsilvered fibres into the cell until the desired particle volume fraction was reached. Prior to the experiments, the fibres were cleaned with soap and water, rinsed with ethanol and with distilled water, and dried, to remove any surface contamination. Typically, about 0.4 g of fibres were silvered.

Eight particle volume fractions were studied for the first batch with $n(l_p/2)^3$ ranging from 0.019 to 2.9 and seven volume fractions for the second batch with $n(l_p/2)^3$ ranging from 0.09 to 13. Therefore both the dilute and the semi-dilute regimes were explored. Additional experiments for the two last batches were performed in the dilute regime.

2.2. *Fibre tracking*

During the experiments, the cell was held in a fixed position on a rail and the cell walls were oriented vertically within 0.05 cm. The cell was illuminated by a set of 5 halogen lights. A 1 cm thick translucent white plastic sheet was placed between the cell and the lights to produce a homogeneous illumination of the suspension. The silvered fibres were tracked with a charged coupled device camera (512×512 pixels) connected to a real time digital imaging system. The intensity of the lights, as well as the camera lens opening, were chosen to ensure the best contrast between the marked fibres and the transparent suspension. The camera was attached to a sliding mount that could be moved along the direction of the vessel height and that was fixed on the rail in front of the cell. The camera was focused on a 1 cm $\times$ 1 cm region in the median plane of the cell (approximately midway between the front and the back walls as well as midway between the sidewalls), referred to as the imaging window. The depth of field of the imaging system was ≈ 2 cm. For all experiments, the diameter of the marked fibres corresponded to 5 pixels.

The experimental procedure was identical for each experiment. The suspension was mixed with a small propeller fixed to the end of a shaft driven by a variable-speed drill motor. The propeller was moved arbitrarily within the suspension in order to obtain a uniform particle distribution throughout the suspension. Care was taken neither to entrain too many air bubbles in the suspension nor to break too many fibres. We checked the homogeneity of the mixing by visually examining the suspension (see § 2.3). The experiments consisted of either tracking a single marked fibre along the vertical direction of the cell through about 10 imaging windows or tracking many marked fibres in a fixed imaging window. The starting time of the tracking ($t = 0$) corresponded to the cessation of mixing. In the first type of experiments, a single marked fibre was tracked first in the upper window, and then, when it reached the window bottom, the imaging system was quickly lowered and the particle was tracked in the next window, which had a small overlap with the upper window to provide measurement continuity, and so on. The imaging windows were located far from the sedimentation front and the sediment layer. In the second type of experiments, any particle entering the fixed window was tracked. The fixed window was located in the middle of the cell height. The experiment was terminated when the sedimentation front reached 4 cm above the marked fibres. The first experimental procedure was very

tedious since only one particle could be tracked per experiment. It was a particularly difficult task at large concentrations because of the large velocity fluctuations which could drive the particles out of the window (see § 3). Conversely, several fibres were tracked in the second procedure. This was a particularly convenient procedure to provide a statistically satisfactory amount of data.

To check whether a convection current existed in the cell containing only the fluid, the trajectory of a nearly buoyant particle was also examined. A small convection current due to a small thermal gradient was found across the cell. It was however of the order of 10^{-4} cm s^{-1} which was an order of magnitude less than the fibre sedimentation speeds.

The imaging system consisted of the video camera connected to a fast and intelligent image processing and acquisition board (Matrox Image 1280), located in a personal computer operating with a digital imaging software package (Visilog 4.1 by Noesis). The tracking was achieved in real time with a specially designed program which allowed the location of the projection of the centre of mass and the measurement of the projection of the orientation of the marked fibre onto the imaging window plane.

The program consisted of the following steps performed for a chosen number of loops which depended upon the duration of the experiment:

(i) image acquisition,

(ii) image threshold for obtaining a binary image in which only the projection of marked fibres onto the window plane could be seen,

(iii) small binary erosion to suppress any small impurities, other than the fibres,

(iv) labelling the objects, i.e. the fibres,

(v) computing the first- and second-order moments of inertia, the surface, and the perimeter of each object,

(vi) computing the horizontal and vertical coordinates of the projected centre of mass, $X_\perp$ and $X_\parallel$ respectively, and the projected angle, ϕ, of the fibre orientation (measured from the horizontal direction) from these moments,

(vii) recording the coordinates, the projected angle, the projected fibre surface and perimeter, and the acquisition time into a file.

By itself, the resolution of the centre of mass provided by the digital imaging application was very precise (≈ 0.2 pixels). However, the image threshold and erosion induced larger errors because of small imperfections in the homogeneity of the cell illumination. This gave a total experimental error in the measurement of the centre of mass of ≈ 2 pixels. The experimental error in the measurement of the projected angle was $\approx 5 \times 10^{-3}$ rad. The sampling time, that is the time between two recordings, had an average value of about 3 s. This sampling time was always smaller than the time a fibre takes to traverse the recording window (at least of the order of 50 s).

The files that contained the projected positions, orientations, surfaces, and perimeters of the marked fibres as a function of time, t, were then analysed with a spreadsheet software (Microsoft Excel 7.0). Specially designed macros (written in Microsoft Visual Basic) allowed discrimination between the different fibres present inside the imaging window and the reconstruction of the fibre centre-of-mass trajectories. Horizontal and vertical instantaneous velocities, $V_\perp$ and $V_\parallel$ respectively, of each fibre were then calculated over each sampling time interval. It was also possible to compute the projected length of the fibre, $l_{projected}$, from the measurement of the projected surface and perimeter and then the cosine of the angle θ between the fibre long axis and the vertical direction as $\cos\theta = l_{projected} \sin\phi / l_p$. The relative error in the measurement of this angle is however very large (at least 20%) because of the large dispersion in fibre length and the large error in surface and perimeter measurements. We therefore

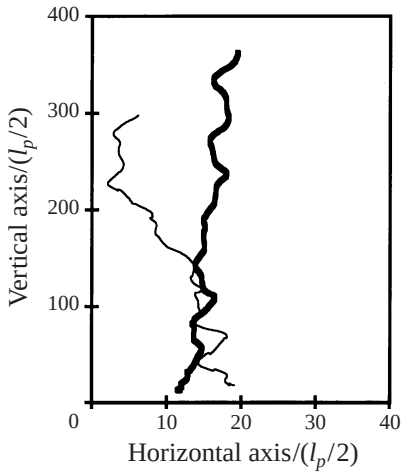

FIGURE 1. Two typical fibre trajectories for $n(l_p/2)^3 = 0.09 \pm 0.03$ and $r = 11 \pm 2$.

chose to present the results in terms of ϕ when possible since its measurement is very precise.

In order to provide a satisfactory data ensemble, a few fibres were tracked over a distance of approximately 10 cm (first type of experiments) and about 1000 fibres over a distance of approximately 1 cm (second type of experiments) for each concentration. We also recorded 30 long fibre trajectories (first type of experiments) at $n(l_p/2)^3 = 0.09 \pm 0.03$ for the first batch in order to investigate the long-time behaviour of the sedimentation process in the dilute regime (see § 3.3).

The general experimental procedure and tracking technique is similar to that used by Nicolai *et al.* (1995) where further details may be found.

2.3. *Visualization of the suspension structure*

In order to examine the structure of the suspension, experiments were performed in a smaller glass-walled cell of rectangular cross-section with an inside width of 6.50 ± 0.05 cm, an inside depth of 3.50 ± 0.05 cm and a height of 40.00 ± 0.05 cm. The fluid and fibres were the same as those of the previous experiment. For low concentrations, all the fibres were silvered. For larger concentrations ($c > 1\%$), since it would have been impossible to see through the suspension if all of the fibres were marked, only about 40% of the fibres were silvered. The structure of the suspension was easily observed when the cell was uniformly lit from behind. The experiment consisted of carefully mixing the suspension and then recording an imaging window of approximately 1 cm $\times$ 1 cm at given intervals of time. The starting time $t = 0$ again corresponded to the cessation of the mixing. The recorded window was located in the middle of the cell, far from the sedimentation front, the sediment layer and the cell walls. The depth of field was chosen to be very small (≈ 0.5 cm) in order to record a vertical sheet of the suspension.

3. Experimental results

3.1. *Influence of the fibre concentration*

The following results are based on experiments performed with a suspension of fibres having an aspect ratio $r = 11 \pm 2$ (batch 1) and for $n(l_p/2)^3$ ranging from 0.019 to 2.9

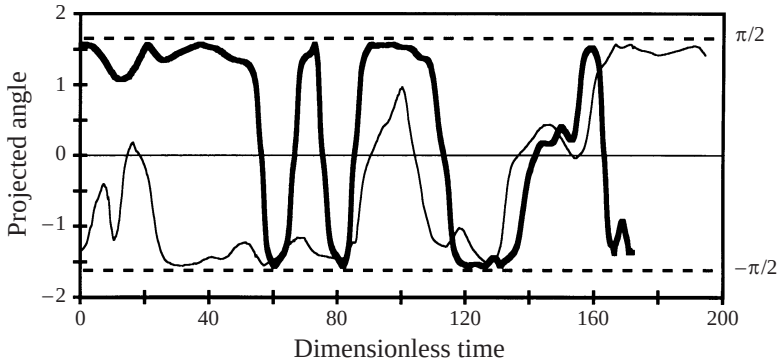

FIGURE 2. Instantaneous projected angles, ϕ, versus dimensionless time, t^*, corresponding to the trajectories of figure 1 ($r = 11 \pm 2$).

(or alternatively c ranging from 0.10% to 15.5%). The trajectories of the fibre centre of mass were found to exhibit large fluctuations as can be seen in figure 1 for $n(l_p/2)^3 = 0.09 \pm 0.03$. The fibre motion fluctuations are strongly anisotropic, with vertical fluctuations much larger than horizontal fluctuations. The corresponding instantaneous projected angles, ϕ, are plotted as a function of time in figure 2. As mentioned earlier, the starting time of fibre tracking ($t = 0$) corresponds to the cessation of the suspension mixing. Here and in the remainder of the paper, all the measured quantities have been made dimensionless with the length scale, $l_p/2$, half the fibre length, and the time scale, $l_p/2V_{S\|}$, the time it takes for a vertical isolated fibre to fall half its length. The dimensionless quantities are labelled by a superscript star (*). After some time, the fibres align in the direction of gravity with occasional flippings between the two possible vertical orientations. It should be mentioned that both fast and slow flipping rotation rates can exist and that there is no periodicity in the flipping motion. This behaviour, i.e. vertical alignment with occasional flippings, was observed for all concentrations.

In order to examine whether a steady state can be achieved, the mean horizontal and vertical velocities, $\langle V_\perp \rangle$ and $\langle V_\| \rangle$ respectively, and the mean absolute value of the projected angles, $\langle |\phi| \rangle$, ensemble averaged over all recorded fibre trajectories were calculated as a function of time for each concentration (see an example in figure 3). This averaging procedure was undertaken over time steps of 4 s. For each time step, the number of instantaneous velocities (or projected angles) used in the statistical ensemble varied between 20 and 100. This number was found sufficient to reduce noticeably the statistical fluctuations. A steady state seemed to be achieved for all the concentrations studied where $\langle V_\perp \rangle^*$ fluctuates around zero and $\langle V_\| \rangle^*$ around values of the order of (or even larger than) 1 for low concentrations and around values lower than 1 for large concentrations. The steady-state time, t_{ss}, i.e. the time it takes for the velocities to reach a steady state, was roughly estimated for each concentration (as an indication, the fluctuations diminish strongly when steady state is reached). Its variation with concentration is given in table 2. It seems that $t_{ss}/(l_p/2\langle V_\| \rangle) \approx 100$ over the studied range of concentration. The mean projected angles, $\langle |\phi| \rangle$, also reached a steady state after even shorter times where they fluctuated around a value ≈ 1.1 rad. It should be noted that this value is smaller than the value of $\pi/2$ rad which corresponds to perfectly aligned fibres because there are always some flipping fibres in the ensemble of data.

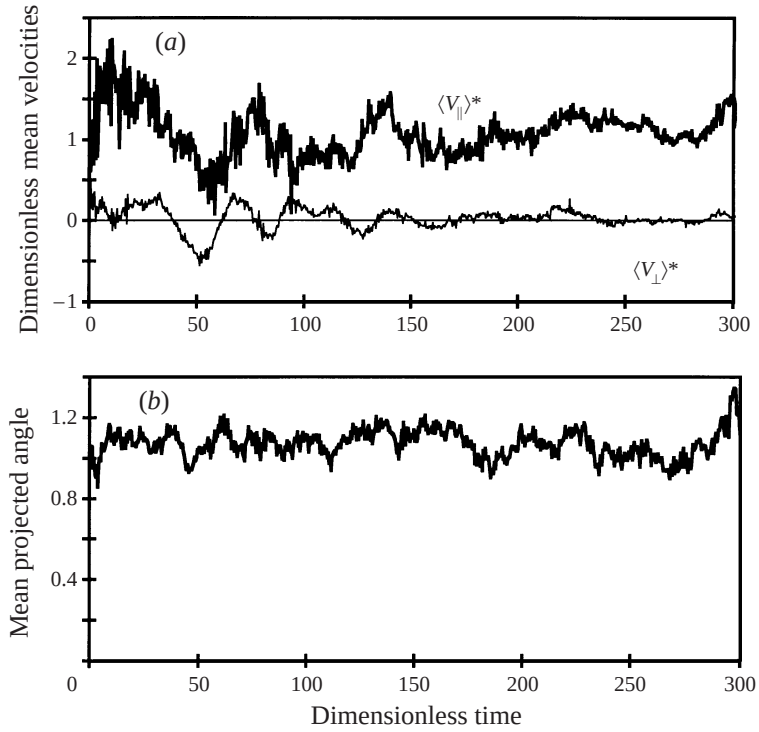

FIGURE 3. (*a*) Dimensionless mean velocities, $\langle V_\perp \rangle^*$ and $\langle V_\parallel \rangle^*$, and (*b*) mean projected angle, $\langle |\phi| \rangle$, versus dimensionless time, t^*, for $n(l_p/2)^3 = 0.05 \pm 0.1$ and $r = 11 \pm 2$.

$n(l_p/2)^3$	0.019 ± 0.006	0.05 ± 0.01	0.09 ± 0.03	0.19 ± 0.06
c (%)	0.10 ± 0.01	0.26 ± 0.01	0.48 ± 0.03	1.03 ± 0.06
t^*_{ss}	100	120	50	110
$\langle V_\perp \rangle^*$	0.029 ± 0.008	0.015 ± 0.006	-0.005 ± 0.005	-0.010 ± 0.006
$\langle V_\parallel \rangle^*$	1.1 ± 0.2	1.1 ± 0.2	1.5 ± 0.3	1.2 ± 0.2
$\sigma^*_\perp$	0.28 ± 0.07	0.28 ± 0.07	0.32 ± 0.08	0.48 ± 0.09
$\sigma^*_\parallel$	0.9 ± 0.2	1.0 ± 0.2	1.1 ± 0.2	1.7 ± 0.3
$\langle 2\cos^2\phi - 1 \rangle$	-0.339 ± 0.004	-0.414 ± 0.004	-0.429 ± 0.004	-0.534 ± 0.003
$n(l_p/2)^3$	0.5 ± 0.1	0.9 ± 0.3	1.4 ± 0.4	2.9 ± 0.9
c (%)	2.5 ± 0.1	4.9 ± 0.3	7.7 ± 0.4	15.5 ± 0.8
t^*_{ss}	100	200	150	200
$\langle V_\perp \rangle^*$	-0.004 ± 0.004	0.015 ± 0.007	0.023 ± 0.006	0.018 ± 0.007
$\langle V_\parallel \rangle^*$	0.9 ± 0.2	0.7 ± 0.1	0.6 ± 0.1	0.23 ± 0.04
$\sigma^*_\perp$	0.61 ± 0.04	0.6 ± 0.1	0.8 ± 0.1	0.7 ± 0.1
$\sigma^*_\parallel$	1.8 ± 0.3	1.7 ± 0.3	2.5 ± 0.4	2.0 ± 0.4
$\langle 2\cos^2\phi - 1 \rangle$	-0.406 ± 0.003	-0.495 ± 0.004	-0.572 ± 0.003	-0.480 ± 0.004

TABLE 2. Steady-state results for fibres having $r = 11 \pm 2$.

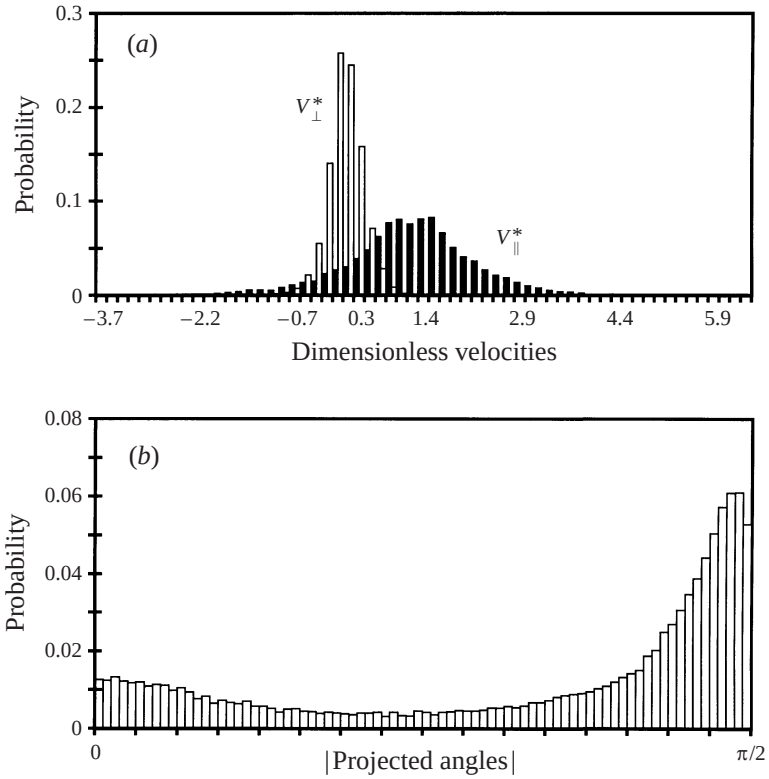

FIGURE 4. Histograms (*a*) of the horizontal (open bars) and vertical (solid bars) dimensionless instantaneous velocities, $V_\perp^*$ and $V_\parallel^*$, and (*b*) of the projected angles, $|\phi|$ for $n(l_p/2)^3 = 0.05 \pm 0.01$ and $r = 11 \pm 2$. The uncertainty is about few percent in each of the orientation bins.

After steady state was reached, we assumed the validity of the ergodic hypothesis. Instantaneous velocities of different fibres were then supposed to be statistically identical to instantaneous velocities of a single fibre along its trajectory. For each concentration, histograms of all instantaneous velocities were computed. The number of data points in each histogram is ≈ 2–5×10^4. Histograms of the velocities were all found to have a strong central tendency, i.e. a tendency to cluster around a definite value, and therefore to be well represented, as a first approximation, by the mean and the variance, as illustrated in figure 4. In order to obtain information regarding the degree of asymmetry of the distributions and their relative peakedness or flatness, we also computed the third and fourth moments of the velocity distribution, i.e. the skewness and the kurtosis, though they are less robust and thus less reliable than the first two moments, i.e. the mean and the variance. The histograms of the horizontal velocities were found to be approximately symmetric (very small skewness) while those of the vertical velocities presented asymmetric tails. These tails extended toward positive or negative values depending upon the concentration without any systematic trend being observed. Both horizontal and vertical histograms were found to be leptokurtic, i.e. slightly peaked, with a kurtosis $\approx$ 5–6 in the horizontal direction and a kurtosis $\approx$ 3–4 in the vertical direction.

The histograms of all projected angles for different fibres were also computed for each concentration in the same manner after steady state has been reached. The histograms of the absolute value of the instantaneous projected angles seem to be

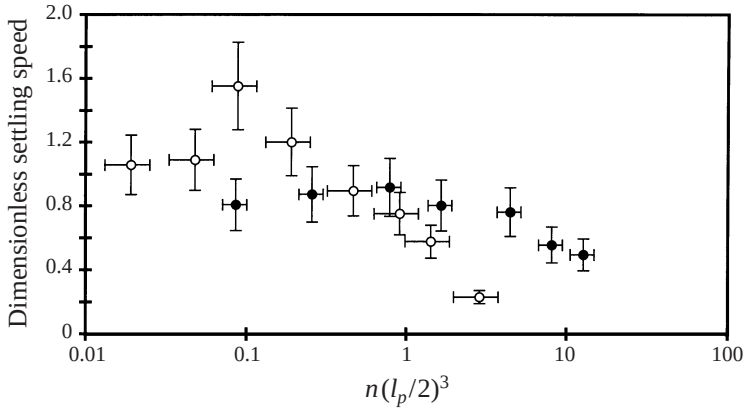

FIGURE 5. Dimensionless settling speed, $\langle V_\parallel \rangle^*$, for $r = 11 \pm 2$ (○) and $r = 32 \pm 4$ (●) versus $n(l_p/2)^3$.

identical for all concentrations (see an example in figure 4). Clearly, the probability for a fibre to align in the direction of gravity is large. There is also a small local maximum around $\phi = 0$. Only about 20% of the data are within $0.3\pi/2$ of the horizontal and more than 40% are within $0.1\pi/2$ of the vertical in the histogram of figure 4. We should mention that the maximum of the distribution is not exactly at $\pi/2$ but at a slightly smaller value for all concentrations. We chose to present the histograms of the instantaneous $|\phi|$ because the histograms of the instantaneous ϕ are perfectly symmetric. E. J. Hinch (private communication) computed the relationship between what was measured here, i.e. the distribution in ϕ, and the physical distribution, i.e. the distribution in the inclination to the vertical θ, by assuming that the distribution for the azimuthal angle is uniform for a given θ. For the results of figure 4, he found that 20% of the fibres are near horizontal in that their vertical projection is less than 30% of their length and that 50% are near vertical in that their vertical projection is more than 90% of their length, as expected from the distribution in ϕ.

Table 2 presents the measured dependence of the dimensionless horizontal and vertical mean velocities, $\langle V_\perp \rangle^*$ and $\langle V_\parallel \rangle^*$ respectively, and the standard deviations, $\sigma_\perp^*$ and $\sigma_\parallel^*$, upon fibre concentration. The experimental errors in the mean and standard deviation were also estimated by computing the usual propagation of errors in simple measurements, such as the instantaneous velocities and sampling time. The statistical error in the mean was also computed as the standard error in the mean. They are probably underestimated since we used the total number of data points instead of the number of uncorrelated data points in the computation. The experimental and statistical errors were found to be of the same order of magnitude, the larger of the two being considered the more representative. The measured mean horizontal velocities were found to be of the order of magnitude of the small thermal convection current (see § 2.2) or to be zero within error bars (the convection current is of the order of magnitude of the uncertainty in the velocity measurements).

The experimental dimensionless settling speeds, $\langle V_\parallel \rangle^*$, are plotted versus $n(l_p/2)^3$ in figure 5. The dimensionless velocity, $\langle V_\parallel \rangle^*$, increases at low concentration to reach a maximum value ≈ 1.5 at $n(l_p/2)^3 \approx 0.1$ and then decreases with increasing $n(l_p/2)^3$ at higher concentration. Clearly, there are two different regimes of sedimentation. At low concentrations, $n(l_p/2)^3 < 0.5$ (or $c < 2.5\%$), the vertical velocity is larger than the Stokes' velocity of an isolated vertical fibre while, at large concentrations, it is hindered.

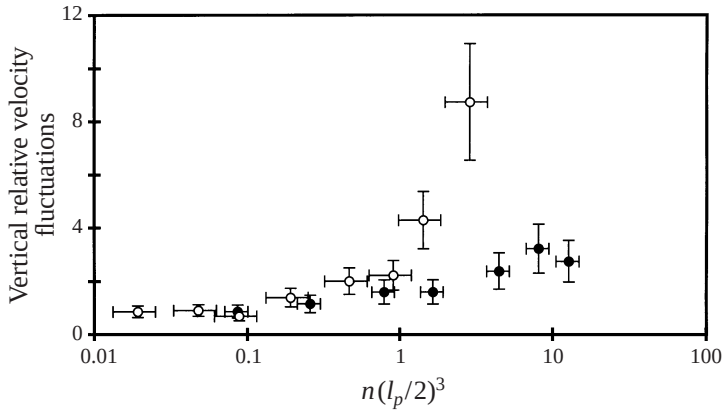

FIGURE 6. Vertical relative velocity fluctuations, $\sigma_\parallel/\langle V_\parallel\rangle$, for $r = 11 \pm 2$ (○) and for $r = 32 \pm 4$ (●) versus $n(l_p/2)^3$.

The dimensionless horizontal and vertical velocity fluctuations, $\sigma_\perp^*$ and $\sigma_\parallel^*$, increase with increasing $n(l_p/2)^3$ in the dilute regime ($n(l_p/2)^3 < 0.5$) and then reach approximately constant values ($\sigma_\perp^* \approx 0.7$ and $\sigma_\parallel^* \approx 2$) at larger concentrations, see table 2. In order to examine the importance of velocity fluctuations, the relative velocity fluctuations in the vertical direction, $\sigma_\parallel/\langle V_\parallel\rangle$, are plotted versus $n(l_p/2)^3$ in figure 6. The relative fluctuations increase with increasing $n(l_p/2)^3$ and can reach extremely large values, ≈ 9 for the largest concentration studied at $n(l_p/2)^3 \approx 2.9$ (or $c \approx 15.5\%$). The fluctuation anisotropy, $\sigma_\parallel/\sigma_\perp$, is constant ≈ 3 for all concentrations.

In order to characterize the degree of anisotropy of the orientation distribution, the two-dimensional 'order parameter' $\langle 2\cos^2\phi - 1\rangle$ was also computed using steady-state data. This 'order parameter' is zero for an isotropic suspension and non-zero for an anisotropic suspension, in particular it is 1 when all the fibres are oriented in a direction perpendicular to gravity and -1 when they are aligned with gravity, see for example the review of Blanc (1995). The 'order parameter' seems to be independent of concentration (see table 2). It has a value ≈ -0.5 for all concentrations, which indicates a substantial anisotropy of the orientation distributions, i.e. a large probability for the fibres to be aligned in a direction close to the vertical direction.

3.2. *Influence of the fibre aspect ratio*

In order to analyse the influence of the fibre aspect ratio on the sedimentation process, we repeated the experiments using a suspension of fibres having a larger aspect ratio $r = 32 \pm 4$ (batch 2) and for $n(l_p/2)^3$ ranging from 0.09 to 13 (or alternatively c ranging from 0.052% to 7.7%). Again, the fibre trajectories were found to present large anisotropic fluctuations and a strong alignment of the fibre with gravity was observed with occasional flippings between the two preferred vertical orientations for all concentrations. A steady state for the mean velocities and the projected angles was also achieved for all the concentrations studied. The dependence of the velocity steady-state time, t_{ss}, on concentration is given in table 3. We found that $t_{ss}/(l_p/2\langle V_\parallel\rangle) \approx 45$ over the studied range of concentrations. The histograms of the instantaneous velocities and projected angles were computed using steady-state data. The remarks made above in § 3.1 are again applicable as far as the general shapes of the histograms are concerned (see an example in figure 7). It is interesting to note that the histograms of $|\phi|$ are very similar whatever the concentrations and aspect ratios are. The 'order param-

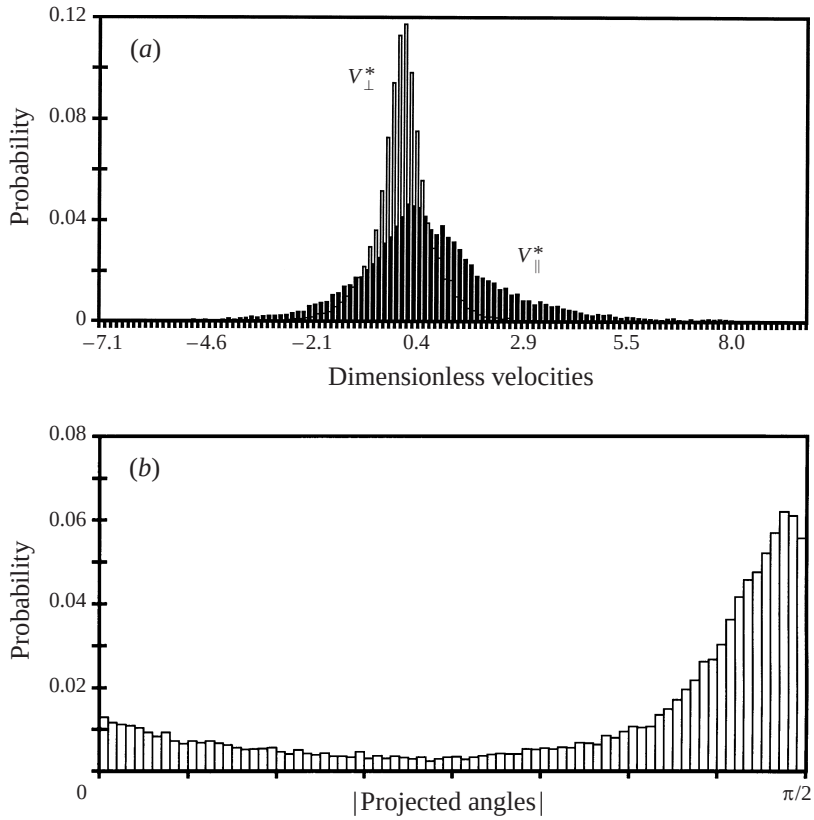

FIGURE 7. As figure 4 but for $n(l_p/2)^3 = 4.5 \pm 0.8$ and $r = 32 \pm 4$.

eter' seems to be independent of concentration and aspect ratio: $\langle 2\cos^2\phi - 1\rangle \approx -0.5$ (see tables 2 and 3). This again shows a substantial alignment of the fibres along directions close to vertical.

The measured dependence of the steady-state dimensionless horizontal and vertical mean velocities, $\langle V_\perp\rangle^*$ and $\langle V_\parallel\rangle^*$ respectively, and standard deviations, $\sigma_\perp^*$ and $\sigma_\parallel^*$, upon fibre concentration is also presented in table 3. Again, we can identify two distinct regimes of sedimentation. At low concentrations, $n(l_p/2)^3 < 4.5$ (or $c < 2.7\%$), the mean velocity is of the order of magnitude of the Stokes' velocity of an isolated vertical fibre (with a small maximum at $n(l_p/2)^3 \approx 0.8$ or $c \approx 0.48\%$) while, at large concentrations, it decreases with increasing concentrations.

To determine the correct scaling for the sedimentation velocity and the velocity fluctuations, the experiments were replicated with a subset of the values of $n(l_p/2)^3$, $n(l_p/2)^2(d_p/2)$ and $n(l_p/2)(d_p/2)^2$ (or c) used previously with the smaller aspect ratio fibres. The dimensionless settling velocity for $n(l_p/2)^3 = 0.09 \pm 0.01$ which corresponded to the maximum velocity (≈ 1.5) for fibres having $r = 11 \pm 2$ (see figure 5) is much smaller ($= 0.8 \pm 0.2$) for the present fibres having $r = 32 \pm 4$. Thus, in the dilute regime, $n(l_p/2)^3$ is not the correct scaling. The dimensionless settling velocity for the present long fibres is also smaller ($= 0.9 \pm 0.2$) for the value of $n(l_p/2)^2(d_p/2)(\approx 0.8\%)$ corresponding to the maximum velocity of the short fibres. Thus, $n(l_p/2)^2(d_p/2)$ is not the correct scaling. Experiments with the same volume fraction as that corresponding to this maximum ($c \approx 0.48\%$) also gave a smaller velocity ($\langle V_\perp\rangle^* = 0.9 \pm 0.2$). The

$n(l_p/2)^3$	0.09 ± 0.01	0.26 ± 0.04	0.8 ± 0.1	1.6 ± 0.3
c (%)	0.052 ± 0.003	0.16 ± 0.01	0.48 ± 0.03	1.00 ± 0.05
t^*_{ss}	60	50	40	65
$\langle V_\perp \rangle^*$	0.000 ± 0.007	0.010 ± 0.008	-0.005 ± 0.009	0.011 ± 0.009
$\langle V_\parallel \rangle^*$	0.8 ± 0.2	0.9 ± 0.2	0.9 ± 0.2	0.8 ± 0.2
$\sigma^*_\perp$	0.29 ± 0.08	0.4 ± 0.1	0.6 ± 0.1	0.5 ± 0.1
$\sigma^*_\parallel$	0.7 ± 0.1	1.0 ± 0.2	1.5 ± 0.3	1.3 ± 0.3
$\langle 2\cos^2\phi - 1 \rangle$	-0.457 ± 0.005	-0.503 ± 0.004	-0.542 ± 0.003	-0.503 ± 0.005
$n(l_p/2)^3$	4.5 ± 0.8	8 ± 1	13 ± 2	
c (%)	2.7 ± 0.1	4.9 ± 0.3	7.7 ± 0.4	
t^*_{ss}	70	80	90	
$\langle V_\perp \rangle^*$	0.013 ± 0.008	-0.001 ± 0.009	0.02 ± 0.01	
$\langle V_\parallel \rangle^*$	0.7 ± 0.2	0.6 ± 0.1	0.5 ± 0.1	
$\sigma^*_\perp$	0.7 ± 0.1	0.7 ± 0.1	0.5 ± 0.1	
$\sigma^*_\parallel$	1.8 ± 0.4	1.8 ± 0.4	1.3 ± 0.3	
$\langle 2\cos^2\phi - 1 \rangle$	-0.494 ± 0.005	-0.480 ± 0.005	-0.534 ± 0.007	

TABLE 3. Steady-state results for the fibres having $r = 32 \pm 4$.

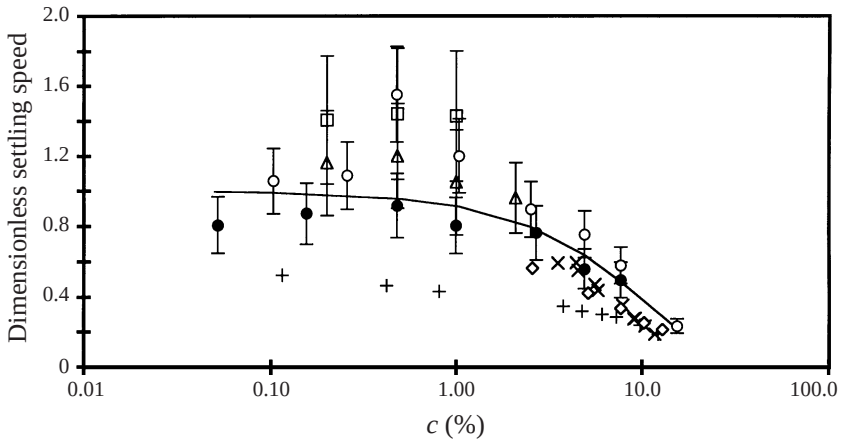

FIGURE 8. Dimensionless settling speed, $\langle V_\parallel \rangle^*$, for $r = 11 \pm 2$ (○), $r = 32 \pm 4$ (●), $r = 20 \pm 3$ (△), and $r = 5 \pm 2$ (□) versus c. Results of Anselmet (1989) for $r = 10$ (+), of Turney *et al.* (1995) for $r = 17.5$ (×), and of the isotropic orientation simulations of Mackaplow & Shaqfeh (1998) (◇). The solid curve corresponds to the Richardson–Zaki law $(1 - c)^9$.

scaling in the dilute regime is therefore complex since none of the dimensionless numbers which can be constructed with n and the two length scales l_p and d_p seems to be sufficient on their own to describe it. It is interesting to note that the maximum velocity for the two aspect ratios seems to occur for the same concentration $c \approx 0.48\%$. It is also important to mention that the dimensionless settling velocity of the long fibres is smaller than that of the short fibres for any given concentration in that dilute regime. The x-axis of figures 5 and 8 (as well as that of figures 6 and 9) has a logarithm scale to spread out the dilute regime.

Conversely, the mean dimensionless settling velocity seems to scale with c at larger concentrations ($c > 1\%$) as can be seen in figure 8. Suspensions having the same

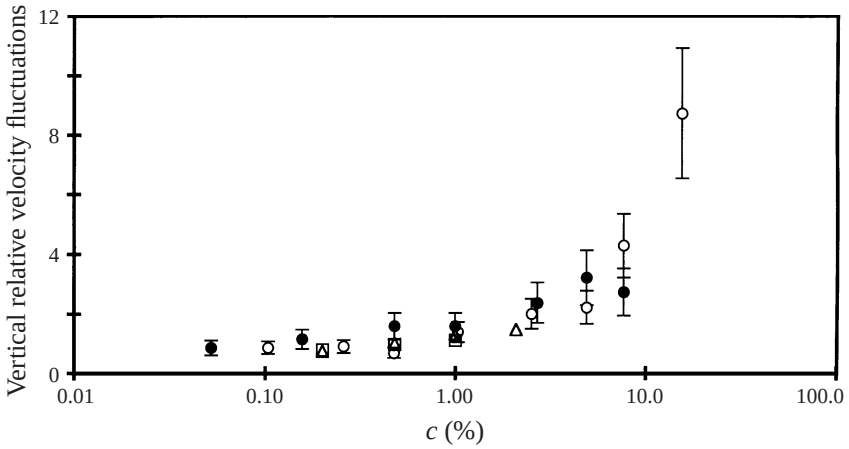

FIGURE 9. Vertical relative velocity fluctuations, $\sigma_\parallel/\langle V_\parallel\rangle$, for $r = 11 \pm 2$ (○), $r = 32 \pm 4$ (●), $r = 20 \pm 3$ (△), and $r = 5 \pm 2$ (□) versus c.

$n(l_p/2)^3$	0.13 ± 0.03	0.30 ± 0.08	0.6 ± 0.2	1.3 ± 0.3
c (%)	0.20 ± 0.01	0.48 ± 0.03	1.00 ± 0.05	2.1 ± 0.1
t^*_{ss}	80	70	80	100
$\langle V_\perp\rangle^*$	0.024 ± 0.008	0.03 ± 0.01	0.02 ± 0.01	0.02 ± 0.01
$\langle V_\parallel\rangle^*$	1.2 ± 0.3	1.2 ± 0.3	1.0 ± 0.3	1.0 ± 0.3
$\sigma^*_\perp$	0.32 ± 0.09	0.4 ± 0.1	0.5 ± 0.1	0.6 ± 0.1
$\sigma^*_\parallel$	0.9 ± 0.2	1.2 ± 0.3	1.3 ± 0.3	1.4 ± 0.4
$\langle 2\cos^2\phi - 1\rangle$	-0.385 ± 0.004	-0.465 ± 0.004	-0.427 ± 0.004	-0.340 ± 0.007

TABLE 4. Steady-state results for the fibres having $r = 20 \pm 3$.

value of c but different values of r settle with the same $\langle V_\parallel\rangle^*$ within error bars. The dimensionless settling velocity clearly does not scale with $n(l_p/2)^3$ or $n(l_p/2)^2(d_p/2)$ as shown in figure 5. The logarithm of the experimental dimensionless velocities for the two aspect ratios has been fitted to a linear function of the logarithm of $1 - c$ by the method of weighted least squares. A Richardson–Zaki law, $\langle V_\parallel\rangle/V_{S\parallel} = (1 - c)^n$, with $n = 9 \pm 2$ is in very good agreement with the experimental data (the correlation coefficient of the linear fit is 0.98).

Again, the velocity fluctuations increase with increasing concentration in the dilute regime and then reach approximately constant values ($\sigma^*_\perp \approx 0.7$ and $\sigma^*_\parallel \approx 1.8$) at larger concentrations (see table 3). The velocity fluctuations seem also to scale with c and not with $n(l_p/2)^3$ nor $n(l_p/2)^2(d_p/2)$ (see tables 2 and 3, and figures 6 and 9). The relative fluctuations increase with increasing concentration as can be seen in figure 9. However, a linear fit (or a linear fit of the logarithms in order to find a power law dependence) does not give a very good correlation coefficient. The fluctuation anisotropy, $\sigma_\parallel/\sigma_\perp$, is again ≈ 3 for the high aspect ratio fibres.

In order to examine in more detail the scaling of the mean velocity in the dilute regime, experiments were performed for two additional fibre aspect ratios, $r = 20 \pm 3$ and $r = 5 \pm 2$ (batches 3 and 4). Again the fibres were found to reach a steady state where they tend to align in the direction of gravity with occasional flipping. Steady-

$n(l_p/2)^3$	0.009 ± 0.004	0.02 ± 0.01	0.04 ± 0.02
c (%)	0.20 ± 0.01	0.48 ± 0.03	1.00 ± 0.05
t^*_{ss}	250	170	200
$\langle V_\perp \rangle^*$	0.05 ± 0.01	0.02 ± 0.01	0.05 ± 0.01
$\langle V_\parallel \rangle^*$	1.4 ± 0.4	1.4 ± 0.4	1.4 ± 0.4
$\sigma^*_\perp$	0.4 ± 0.1	0.5 ± 0.1	0.5 ± 0.1
$\sigma^*_\parallel$	1.1 ± 0.3	1.4 ± 0.4	1.6 ± 0.4
$\langle 2\cos^2\phi - 1 \rangle$	-0.224 ± 0.002	-0.298 ± 0.002	-0.303 ± 0.002

TABLE 5. Steady-state results for the fibres having $r = 5 \pm 2$.

state results are reported in tables 4 and 5. The mean velocity data for $r = 20 \pm 3$ lie between those for $r = 11 \pm 2$ and $r = 32 \pm 4$ as can be seen in figure 8. For $r = 5 \pm 2$, the mean velocities are about 1.4. The uncertainties for this smallest aspect ratio are very large because of the large variation in fibre lengths. It should be mentioned that, for this last aspect ratio, the orientation order parameter is smaller than for the other aspect ratios (see table 5). The relative velocity fluctuations seem to scale with c (see figure 9).

3.3. *Long-time behaviour in the dilute regime*

In order to determine the long-time behaviour of the fluctuating fibre motions, it was necessary to record very long fibre trajectories. As mentioned in § 2.2, tracking a fibre over a long distance (first type of experiments) was very difficult and tedious because of the large velocity fluctuations which can drive particles out of the imaging window. This became nearly impossible at large concentrations because the velocity fluctuations grew to be much larger than the mean. Long-distance fibre tracking was thus performed in the dilute regime for a concentration where the fluctuations were of the order of the mean. We recorded 30 long fibre trajectories at $n(l_p/2)^3 = 0.09 \pm 0.03$ ($c = 0.48 \pm 0.03\%$) in a suspension of fibres having $r = 11 \pm 2$ (batch 1). This concentration corresponds roughly to the maximum velocity obtained in the dilute regime (see figures 5 and 8).

In order to examine whether velocity fluctuations of the centre of mass of the fibres become uncorrelated, velocity fluctuation autocorrelation functions were computed. Since the sampling time slightly varied along a particle trajectory, the coordinates of the centre of mass were first linearly interpolated for constant intervals (= 2 s). The horizontal and vertical instantaneous translational velocities were then calculated over each interval. The horizontal and vertical velocity fluctuation autocorrelation functions, denoted $C(t)$ ($C_\perp$ and $C_\parallel$ respectively), were therefore computed as $C(t) = \langle V'(t_0)V'(t_0 + t)\rangle$ ensemble averaged over different fibre trajectories and different starting times t_0 along the trajectory. Here $V' = V - \langle V \rangle$ is the instantaneous velocity fluctuation where $\langle V \rangle$ is the mean velocity calculated for the 30 chosen fibres. This number of 30 fibres was found sufficient to reduce noticeably the statistical fluctuations. The errors in the correlation functions were given by the standard errors, i.e. the 68% confidence limits. Normalized velocity fluctuation autocorrelation functions, $C(t)/C(0)$, for both horizontal and vertical directions, are shown in figure 10. The correlation functions always decrease toward zero, which demonstrates that the translational velocities of the fibre always become uncorrelated. Moreover, the horizontal function decays more rapidly than the vertical function. When the functions

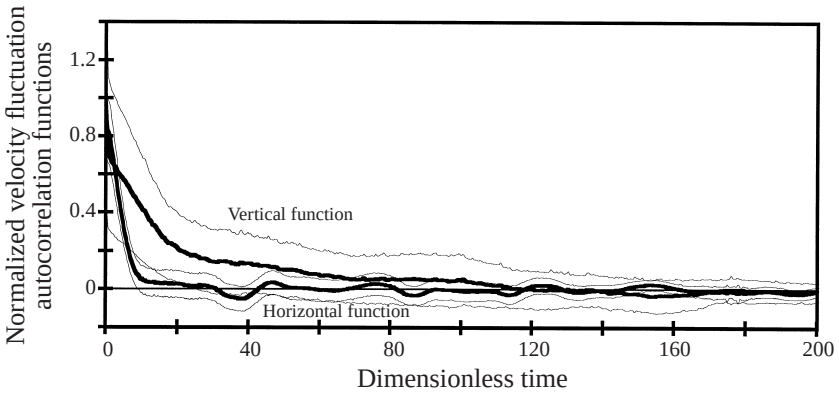

FIGURE 10. Normalized velocity fluctuation autocorrelation functions (bold curves) for the horizontal and vertical directions versus dimensionless time, t^*, for $n(l_p/2)^3 = 0.09 \pm 0.03$ and $r = 11 \pm 2$. The thin curves correspond to the 68% confidence limits.

$t^*_{c\perp}$	Integral method	4 ± 1
$D^*_\perp$	Integral method	0.3 ± 0.1
$D^*_\perp$	Second-order moment method	0.3 ± 0.1
$t^*_{c\parallel}$	Integral method	16 ± 8
$D^*_\parallel$	Integral method	16 ± 5
$D^*_\parallel$	Second-order moment method	12 ± 4

TABLE 6. Dimensionless horizontal and vertical centre-of-mass correlation times and self-diffusivities for $n(l_p/2)^3 = 0.09 \pm 0.03$ and $r = 11 \pm 2$.

approach zero, the oscillations around zero are due to statistical noise. Horizontal and vertical correlation times, $t_{c\parallel}$ and $t_{c\perp}$, were calculated as $t_c = [1/C(0)] \int_0^\infty C(t)\mathrm{d}t$. In practice, the upper bound of the integral corresponds to the time at which $C(t)$ began to oscillate around zero. The anisotropy in the correlation time, $t_{c\parallel}/t_{c\perp}$, is large ≈ 4 (see table 6).

The diffusive behaviour of the motion fluctuations of the centre of mass of the fibre was established by two means. First, integrals of the correlation functions were shown to reach saturation values which are defined as the self-diffusivities, $D = \int_0^\infty C(t)\ \mathrm{d}t = C(0)\ t_c$, as can be seen in figure 11. It should be mentioned that, in order to prevent the few observations at large time separations dominating this integral, the velocity correlation function was defined in a slightly different way as $C(t) = \sum_{fibres,t_0} V'(t_0)V'(t_0+t)/\sum_{fibres}$(number of data points at $t = 0$), see Nicolai *et al.* (1995) for further details. Secondly, the second-order moments of the particle displacement fluctuations, computed as $\langle(X(t_0+t)-X(t_0)-\langle V\rangle t)^2\rangle$ ensemble averaged over the same set of long trajectories and different starting times t_0, were found to grow linearly with time after a few correlation times (see figure 12). The self-diffusivity is estimated as half the slope of this linear growth. The self-diffusivities estimated with the different methods match within error bars (see table 6). The self-diffusion process of the centre of mass of the fibre is strongly anisotropic, $D_\parallel/D_\perp \approx 50$.

In order to examine whether the fibre orientation became uncorrelated, orientation autocorrelation functions were also computed. The projected angle autocorrelation

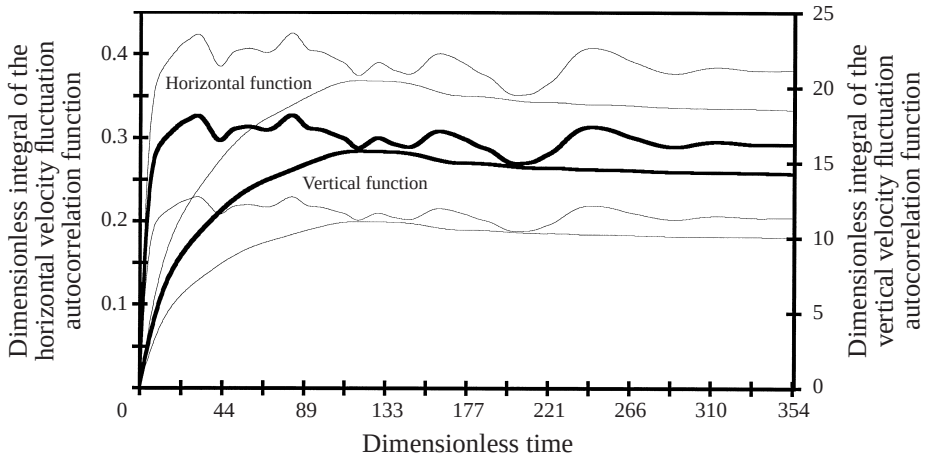

FIGURE 11. Dimensionless integrals of the velocity fluctuation autocorrelation functions (bold curves) for the horizontal and vertical directions versus dimensionless time, t^*, for $n(l_p/2)^3 = 0.09 \pm 0.03$ and $r = 11 \pm 2$. The thin curves correspond to the 68% confidence limits.

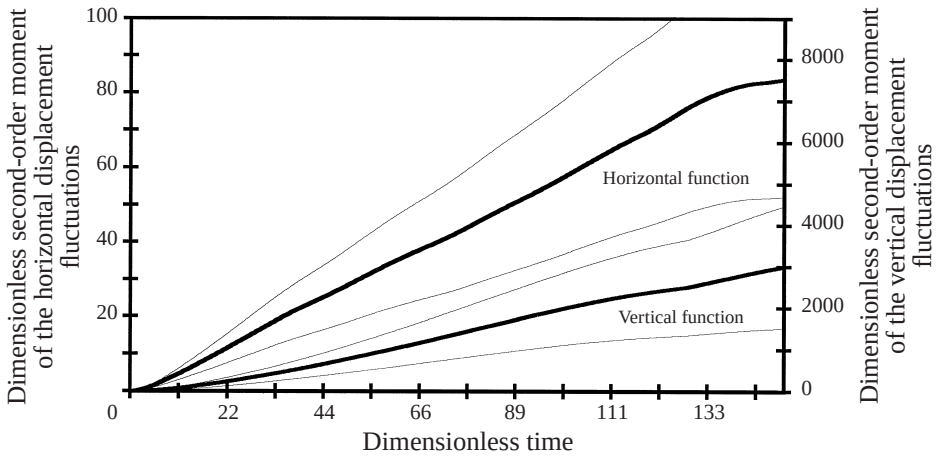

FIGURE 12. Dimensionless second-order moments of the particle displacement fluctuations (bold curves) for the horizontal and vertical directions versus dimensionless time, t^*, for $n(l_p/2)^3 = 0.09 \pm 0.03$ and $r = 11 \pm 2$. The thin curves correspond to the 68% confidence limits.

function was computed as $\langle \phi'(t_0)\ \phi'(t_0 + t)\rangle$ where $\phi' = |\phi| - \langle|\phi|\rangle$. Since the orientation can also be characterized by the second Legendre polynomial $P_2(\cos\theta) = (3\cos^2\theta - 1)/2$ where θ is the angle between the long axis of the fibre and gravity, the $P_2(\cos\theta)$ autocorrelation function was also computed in the same manner as $\langle P_2(\cos\theta)(t_0)P_2(\cos\theta)(t_0 + t)\rangle$. Both correlation functions decay toward zero with a relaxation similar to that of the vertical translational velocity correlation function (the dimensionless correlation time for the $P_2(\cos\theta)$ autocorrelation function is 16 ± 5, see figure 13). We also computed the angular velocity autocorrelation function as $\langle \mathrm{d}\phi/\mathrm{d}t(t_0)\ \mathrm{d}\phi/\mathrm{d}t(t_0 + t)\rangle$, the mean rotational velocity being zero within error bars. The angular velocities of the projected angle were found to become very rapidly uncorrelated after a dimensionless time ≈ 1. However, the long-time behaviour of

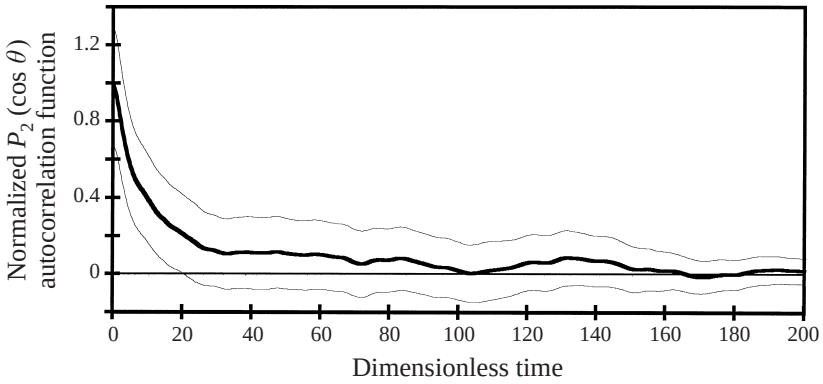

FIGURE 13. Normalized $P_2(\cos\theta)$ autocorrelation function (bold curve) versus dimensionless time, t^*, for $n(l_p/2)^3 = 0.09 \pm 0.03$ and $r = 11 \pm 2$. The thin curves correspond to the 68% confidence limits.

the angle was not found to be diffusive. Indeed, the second-order moment of the orientation fluctuations does not grow linearly with time.

Finally, crosscorrelation functions between centre-of-mass velocities and angular velocities (or orientations) were also computed and no significant correlation was observed.

3.4. *Structure of the suspensions*

Visualizations of the suspension structure were undertaken with the use of the technique described in § 2.3. Figure 14 presents two images of the suspension structure at two different times for $r = 11 \pm 2$ and $c = 0.48 \pm 0.03\%$. Figure 15 presents two images of the suspension for $r = 32 \pm 4$ at the same volume fraction and dimensionless times. A short time after cessation of mixing, the suspension seems to be well mixed and rather homogeneous (see figures 14*a* and 15*a*). At longer times, the suspension becomes inhomogeneous. The fibres clump and form slightly elongated packets separated by sparse regions of the suspension (see figures 14*b* and 15*b*). A steady state seems to be reached where the packets no longer grow in size. There is clearly a wide distribution of packet sizes with a maximum dimension of a few fibre lengths. Video movies made with our experimental system show that the packets are constantly breaking up and forming, i.e. capturing and loosing fibres. Fibres are peeled off from the sides of the packets (or in their wake) by the shear created by the fluid rising in the less dense areas. Packets capture fibres in front of them as they settle. They settle at large velocities and the fibres align in their wake. The same qualitative behaviour in the dilute regime, i.e. the structure instability, is observed for the two different aspect ratios, although the dimensionless mean velocity is lower for the larger aspect ratio.

Visualizations were also undertaken in the concentrated regime ($c = 1.8\%$), but only 40% of the fibres were marked. Pictures and movies do not show a clear evolution of the structure with time. Denser areas form in the suspension but seem to stay connected to one another. Indeed, fibres seem to form a loose connected network and the fluid backflow goes up through openings in this network. Video movies show that very large collective motions exist in the suspension, which is consistent with the very large velocity fluctuations observed in this regime.

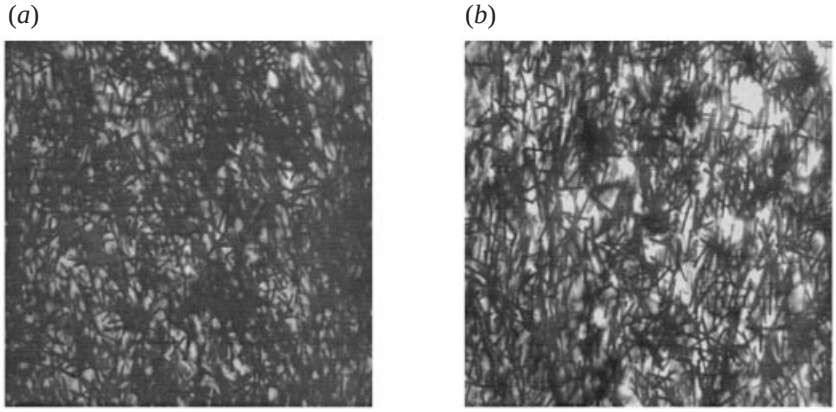

FIGURE 14. Photographs of the suspension structure for $r = 11 \pm 2$ and $c = 0.48 \pm 0.3\%$: (*a*) $t^* \approx 5$ and (*b*) $t^* \approx 60$.

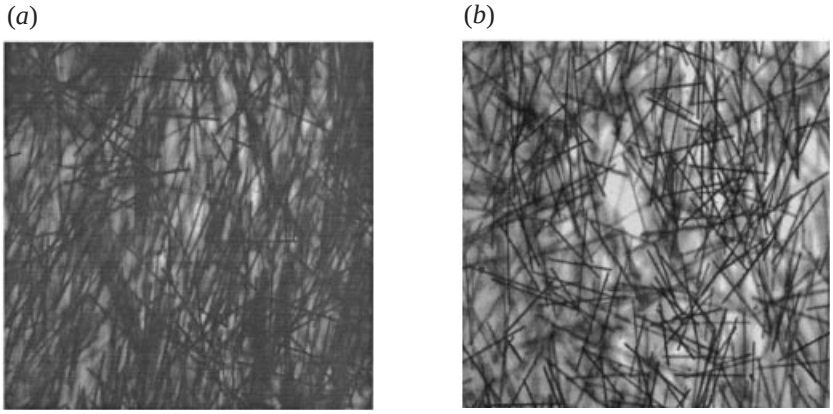

FIGURE 15. Photographs of the suspension structure for $r = 32 \pm 4$ and $c = 0.48 \pm 0.3\%$: (*a*) $t^* \approx 5$ and (*b*) $t^* \approx 60$.

4. Discussion and conclusions

The sedimentation of fibre suspensions having different aspect ratios has been studied experimentally under Stokes' flow conditions. A few marked fibres were tracked in the bulk of a suspension of like fibres, using a real time digital imaging system. Fibre trajectories and orientations were examined in both the dilute and the semi-dilute regimes.

The fibre trajectories were found to present large anisotropic fluctuations and a substantial alignment of the fibres with gravity was observed with occasional flippings between the two preferred vertical orientations for all concentrations and aspect ratios studied. A steady state for the mean settling velocity and the orientation was always achieved. Two different steady-state regimes of sedimentation were clearly identified. The mean settling velocity was found to increase at low concentrations, to reach a maximum value (more or less pronounced depending upon the aspect ratios) at a volume fraction $c \approx 0.48\%$ and then to decrease with increasing concentrations at higher concentration.

In the dilute regime, the steady-state suspension was observed to be a very inhomogeneous suspension in which fibre packets settle faster than an isolated fibre would

do. This leads to a settling velocity which is not hindered and which in fact can be larger than the Stokes' velocity of an isolated vertical fibre, i.e. the maximum possible value for a fibre in Stokes' flow. The scaling of the dimensionless velocity in this dilute regime is complex since none of the dimensionless numbers $n(l_p/2)^3$, $n(l_p/2)^2 d_p$, and $n(l_p/2)(d_p/2)^2$ (or alternatively c) seems to be sufficient on their own to describe it. The velocity seems to be a function of both c and r, $\langle V_\parallel \rangle / V_{S\parallel} = f(c, r)$. The function of r is complicated: it increases first with r, reaches a maximum for $r \approx 5$–15 and then decreases at large r. This seems to indicate that the magnitude of the instability decreases at high aspect ratios.

These findings confirm and extend the observations of Herzhaft *et al.* (1996). The present work clearly identifies a dilute regime in which a well-stirred suspension of fibres is unstable. In this regime, the fibres align in the direction of gravity and clump together to form packets. Since the packets continuously capture and lose fibres, they stop growing in size and there is clearly a wide distribution of packet sizes. The large shear stresses between the different sparse and dense regions of the suspension seems to be (at least partly) responsible for the flipping motion of the fibres. The existence of the instability of a dilute sedimenting suspension of fibres was predicted by Koch & Shaqfeh (1989). It should be mentioned that Hinch (1988) came to a different conclusion. He found that the fibres should disperse. The present experiment demonstrates the existence of an instability but cannot prove that the argument of Koch & Shaqfeh (1989) is correct. Also, the linear stability analysis of Koch & Shaqfeh (1989) cannot predict the steady-state settling velocity, fibre orientation distribution, and structure achieved by the settling suspension. The present experimental results are in qualitative agreement with the point fibre dynamic simulations of Mackaplow & Shaqfeh (1998) as far as the occurrence of the instability and the fibre flippings are concerned. However, the settling velocity and the fibre clumping did not stop growing with time in these simulations. Therefore, unlike in the experiments, steady state is not reached in the simulations. The only previous experimental results available in the dilute regime are those of Anselmet (1989). Although two different regime of sedimentation were identified as in the present work, the measured settling velocities were found to be much lower than the present estimates (see figure 8). This may be due to the small size of her experimental vessel which prevented the steady state being completely reached.

To complete the discussion, it is also important to examine whether non-hydrodynamic interactions can exist among the fibres and be responsible for clumping. Electric double layers do not occur in the non-ionic organic fluid used in the experiments. The fibres are too large for Van der Waals forces to have any effect. (Moreover, the optical index-matching will reduce the contributions to the Hamaker constant from the visible range, if not more). There is no capillary effect (for instance due to microbubbles on the surface of the fibres). The formation of fibre packets thus seems to be a purely hydrodynamic effect. Qualitative experiments with nylon fibres (of approximately the same size as that of the glass fibres used here) in water show clustering in a length scale of about one fibre length. This suggests that fibre clumping can be seen with other types of fibres and fluids.

In this dilute regime, we have also examined the long-time behaviour of the fluctuating fibre motion. The long-time fluctuating motion of the fibre centre of mass was demonstrated to be diffusive in nature and a strong anisotropic diffusion noted. Conversely, although the orientation and the rotational velocity became uncorrelated, the long-time behaviour of the orientation was not found to be diffusive. This behaviour may be due to large steps such as the fibre flippings which decorrelate the

rotational velocity but do not lead to a long-time diffusion process (one needs lots of uncorrelated small steps to be diffusive). No correlation was found between the centre-of-mass velocity and the orientation. This finding suggests that hydrodynamic interactions dominate the coupling between centre-of-mass and orientational motion which exists for an isolated fibre.

As the concentration was increased ($c > 1\%$), we observed that the fibres still tend to orient in the direction of gravity and the mean velocity becomes hindered. The fibres seem to be all connected like in a loose packing and large collective motions were observed. The mean settling velocity was found to scale with c in this regime. A Richardson-Zaki law, $\langle V_{\parallel}\rangle / V_{S\parallel} = (1-c)^n$ with $n = 9 \pm 2$, is in very good agreement with the experimental data. The following considerations can give some clues to the observed scaling. Since the fibres are strongly aligned in the direction of gravity, they cannot take all the orientations on the effective sphere of radius $l_p/2$ and therefore it is not the effective volume fraction $n(l_p/2)^3$ which is the important parameter. The governing parameter is then the real volume fraction c of the fibres and the major mechanism for hindrance is therefore the fluid backflow as in a sedimenting suspension of spheres, see Batchelor (1972).

The present results in this second regime are in good agreement with the measurements of Turney *et al.* (1995), though slightly larger (see figure 8). These results are also of the same order of magnitude as the predictions of the Monte Carlo simulation of Mackaplow & Shaqfeh (1998). This last comparison should be handled carefully since the simulation assumes that the suspension is homogeneous and has an isotropic orientation distribution. It should also be mentioned that recent experimental measurements of the settling interface speed by A. Ratiarison & R. Blanc (private communication) also show that the volume fraction c is the correct scaling in the semi-dilute regime. The results of Ratiarison & Blanc for fibre suspensions having $r = 12.2, 18.6, 21.6$ and 26.5 are in very good agreement with the present data.

The velocity fluctuations have been found to increase with increasing concentrations in the dilute regime and then to reach approximately constant values at larger concentrations. The relative fluctuations increase with increasing concentrations and seem to scale with c. The dependence of the relative fluctuations on c seems to be a more complex function than a linear variation or a power law. The relative fluctuations can reach extremely large values, $\approx 900\%$ for the largest concentration studied. The fluctuation anisotropy is independent of concentration and aspect ratio and has a value ≈ 3.

An important finding of the present work is that the orientation distributions are quite similar whatever are the concentrations and aspect ratios. There is a substantial alignment of the fibres along directions close to the vertical direction. There is also always a smaller tendency to align near horizontal which is at present not explained. To characterize the degree of anisotropy of the orientation distributions, we computed the two-dimensional 'order parameter' $\langle 2\cos^2\phi - 1\rangle$ and found that it is independent of concentration and aspect ratio. It has a value ≈ -0.5, which indicates a substantial anisotropy of the orientation distribution. It also suggests that the fibres are not really flipping in Jeffery (1922)'s orbits as in a vertical shear flow since that would produce a stronger alignment with increasing aspect ratio.

We would like to thank R. Blanc, E. J. Hinch, D. L. Koch, M. B. Mackaplow, and E. S. G. Shaqfeh for helpful discussions during the course of this work. This work is part of the thesis of B. Herzhaft sponsored by the Ministère de l'Éducation, de la Recherche et de la Technologie. It was also undertaken under the auspices of the

Groupement de Recherche du CNRS 'Physique des Milieux Hétérogènes Complexes', the European network 'Cooperative Phenomena in Complex Systems', and the CNRS-NSF Cooperative Research Project 'Fundamental studies of suspensions of anisotropic particles'. The Santicizer 97 and Santicizer 431 were donated by Monsanto. We also thank E. S. G. Shaqfeh for providing the first two batches of glass fibres manufactured by Mo-Sci Corporation. Finally, special recognition and thanks must be given to T. Duhaut for his assistance in performing some of the experiments during his undergraduate stay in our laboratory.

REFERENCES

Anselmet, M.-C. 1989 Contribution à l'étude des systèmes fluide-particules : suspensions de cylindres, lits fluidisés. Thèse, Université de Provence.

Batchelor, G. K. 1970 Slender-body theory for particles of arbitrary cross-section in Stokes flow. *J. Fluid Mech.* **44**, 419–440.

Batchelor, G. K. 1972 Sedimentation in a dilute dispersion of spheres. *J. Fluid Mech.* **123**, 245–268.

Blanc, R. 1995 Order and disorder in fiber suspensions. In *Mobile Particulate Systems* (ed. E. Guazzelli & L. Oger), pp. 105–128. Kluwer.

Caflisch, R. E. & Luke, J. H. C. 1985 Variance in the sedimenting speed of a suspension. *Phys. Fluids* **28**, 759–760.

Claeys, I. L. & Brady, J. F. 1993 Suspensions of prolate spheroids in Stokes flow. Part 3. Hydrodynamic transport properties of crystalline dispersions. *J. Fluid Mech.* **251**, 479–500.

Da Cunha, F. R. 1994 *Hydrodynamic dispersion in suspensions.* Ph.D thesis, University of Cambridge.

Davis, R. H. & Acrivos, A. 1985 Sedimentation of noncolloidal particles at low Reynolds number. *Ann. Rev. Fluid Mech.* **17**, 91–118.

Ham, J. M. & Homsy, G. M. 1988 Hindered settling and hydrodynamic dispersion in quiescent sedimenting suspension. *Intl J. Multiphase Flow* **14**, 533–546.

Hasimoto, H. 1959 On the periodic fundamental solutions of the Stokes equations and their application to a viscous flow past a cubic array of spheres. *J. Fluid Mech.* **5**, 317–328.

Herzhaft, B., Guazzelli, É., Mackaplow, M. B. & Shaqfeh, E. S. G. 1996 Experimental investigation of the sedimentation of a dilute fiber suspension. *Phys. Rev. Lett.* **77**, 290–293.

Hinch, E. J. 1988 Sedimentation of small particles. In *Disorder and Mixing* (ed. E. Guyon, J.-P. Nadal & Y. Pomeau), pp. 153–161. Kluwer.

Jeffery, G. B. 1922 The motion of ellipsoidal particles immersed in a viscous fluid. *Proc. R. Soc. Lond.* A **102**, 161–179.

Koch, D. L. 1994 Hydrodynamic diffusion in a suspension of sedimenting point particles with periodic boundary conditions. *Phys. Fluids* **6**, 2894–2900.

Koch, D. L. & Shaqfeh, E. S. G. 1989 The instability of a dispersion of sedimenting spheroids. *J. Fluid Mech.* **209**, 521–542.

Koch, D. L. & Shaqfeh, E. S. G. 1991 Screening in sedimenting suspensions. *J. Fluid Mech.* **224**, 275–303.

Kumar, P. & Ramarao, B. V. 1991 Enhancement of the sedimentation rates in fibrous suspensions. *Chem. Engng Commun.* **108**, 381–401.

Ladd, A. J. C. 1997 Sedimentation of homogeneous suspensions of non-Brownian spheres. *Phys. Fluids* **9**, 491–499.

Mackaplow, M. B. 1996 A study of the transport properties and sedimentation characteristics of fiber suspensions. Ph.D thesis, Stanford University.

Mackaplow, M. B. & Shaqfeh, E. S. G. 1998 A numerical study of the sedimentation of fibre suspensions. *J. Fluid Mech.* **376**, 149–182.

Nicolai, H. & Guazzelli, E. 1995 Effect of the vessel size on the hydrodynamic diffusion of sedimenting spheres. *Phys. Fluids* **7**, 3–5.

Nicolai, H., Herzhaft, B., Hinch, E. J., Oger, L. & Guazzelli, E. 1995 Particle velocity fluctuations and hydrodynamic self-diffusion of sedimenting non-Brownian spheres. *Phys. Fluids* **7**, 12–23.

Rahnama, M., Koch, D. L. & Shaqfeh, E. S. G. 1995 The effect of hydrodynamic interac-

tions on the orientation distribution in a fiber suspension subject to simple shear flow. *Phys. Fluids* **7**, 487–506.

Richardson, J. F. & Zaki, W. N. 1954 Sedimentation and fluidization: Part I. *Trans. Inst. Chem. Engrs* **32**, 35–53.

Russel, W. B., Hinch, E. J., Leal, L. G. & Tieffenbruck, G. 1977 Rods falling near a vertical wall. *J. Fluid Mech.* **83**, 273–287.

Saffman, P. G. 1973 On the settling speeds of free and fixed suspensions. *Stud. Appl. Maths* **52**, 115–127.

Sangani, A. S. & Acrivos, A. 1982 Slow flow through a periodic array of spheres. *Intl J. Multiphase flow* **8**, 343–360.

Segrè, P. N., Herbolzheimer, E. & Chaikin, P. M. 1997 Long-range correlations in sedimentation. *Phys. Rev. Lett.* **79**, 2574–2577.

Shaqfeh, E. S. G. & Koch, D. L. 1988 The effect of hydrodynamic interactions on the orientation of asymmetric particles flowing through a fixed bed of spheres or fibers. *Phys. Fluids* **31**, 728–743.

Turney, M. A., Cheung, M. K., McCarthy, M. J. & Powell, R. L. 1995 Hindered settling of rod-like particles measured with magnetic resonance imaging. *AIChE J.* **41**, 251–257.

Xue, J. Z., Herbolzheimer, E., Rutgers, M. A., Russel, W. B. & Chaikin, P. M. 1992 Diffusion, dispersion and settling of hard spheres. *Phys. Rev. Lett.* **69**, 1715–1718.

Youngren, G. K & Acrivos, A. 1975 Stokes flow past a particle of arbitrary shape: a numerical method of solution. *J. Fluid Mech.* **69**, 377–403.